Petroleum Science 18 (2021) 1305–1322

Contents lists available at ScienceDirect

Petroleum Science

journal homepage: www.keaipublishing.com/en/journals/petroleum-science

Original Paper

Study on the relationship between hydrocarbon generation and pore evolution in continental shale from the Ordos Basin, China

Ji-Yuan Wang [a, b], Shao-Bin Guo [a, b, *]

[a] School of Energy Resources, China University of Geosciences, Beijing, 100083, China
[b] Key Laboratory of Strategy Evaluation for Shale Gas, Ministry of Land and Resources, Beijing, 100083, China

ARTICLE INFO

Article history:
Received 5 October 2020
Accepted 26 January 2021
Available online 21 August 2021

Edited by Jie Hao

Keywords:
Shale
Hydrocarbon generation
Pore evolution
Fractal dimension

ABSTRACT

The relationship between hydrocarbon generation and the evolution of shale pore structure and its heterogeneity of continental shale from the Ordos Basin, China was quantitatively studied based on thermal simulation experiment, mercury injection capillary pressure (MICP), gas adsorption, vitrinite reflectance (R_o) analysis, and hydrocarbon generation test combined with Frenkel-Halsey-Hill (FHH) fractal model. The result shows that the pore volume (PV) and specific surface area (SSA) of pores with different pore sizes show a trend of decreasing first and then increasing as the maturity increases in general, R_o>1.59% is initially defined as a favorable stage for pore development in continental shale. Hydrocarbon generation has different effects on pore heterogeneity of different scales. For the N_2 adsorption, the roughness of small pore surface (D_1) decreases in the oil window; the complexity of large pore structure (D_2) increases in the oil window but decreases in the gas window. For the MICP, the heterogeneity of small pore (D_1) increases in the oil window and increases first and then decreases in the gas window; D_2 remains basically constant during the whole stage and is close to 3, indicating that the heterogeneity of large pores is extremely strong and is not affected by hydrocarbon generation.

1. Introduction

As a kind of self-generating and self-storing unconventional resource, shale gas has been a focus in the current research. Different from conventional oil and gas, shale gas is stored directly in the pores of the shale without being transported. Therefore, it is crucial to study the pore structure and its evolution characteristics of shale (Ross and Bustin, 2009; Loucks et al., 2009; Chalmers et al., 2012; Clarkson et al., 2013). Pores of shale can be subdivided into micropores (pore width <2 nm), mesopores (pore width between 2 and 50 nm) and macropores (pore width >50 nm) according to the classification of International Union of Pure and Applied Chemistry (IUPAC) (Sing et al., 1985). Previous studies have confirmed that shale gas mainly exists in the pores of shale in free and adsorbed states, and the pore structure of shale is the main factor controlling the occurrence of them (Ross and Bustin, 2007; Jarvie et al., 2007; Chalmers and Bustin, 2008). Several methods have been successfully used to characterize the complex pore systems of shale. Scanning electron microscopy (SEM) is the most commonly technique to qualitatively identify shale pores (Curtis et al., 2012; Gu et al., 2015). MICP, low pressure gas adsorption experiments are used to quantitatively characterize shale pores (Cui et al., 2012; Zhao and Guo, 2015; Tang et al., 2016). The rise of thermal simulation experiment realizes the dynamic characterization of shale pore structure in the laboratory (Chen and Xiao, 2014; Sun et al., 2015; Ma et al., 2017; Ko et al., 2018).

Shale has experienced complex geological evolution in its natural state, and the thermal evolution process with maturity as the main indicator is the period of hydrocarbon generation and the important stage of pore evolution. In recent years, more and more scholars have paid attention to the relationship between them. Guo et al. combined thermal simulation experiment with X-ray diffraction, SEM, MICP, and gas adsorption experiments to carry out dynamic characterization of pore evolution of the marine-continental transitional facies shale in the Shanxi Formation of the Ordos Basin. They concluded that the PV and SSA of shale initially decreased and then increased with the increase of maturity (Guo and Mao, 2019). Wang et al. used thermal simulation

* Corresponding author. School of Energy Resources, China University of Geosciences, Beijing, 100083, China.
E-mail address: guosb58@cugb.edu.cn (S.-B. Guo).

https://doi.org/10.1016/j.petsci.2021.01.002

experiment, gas adsorption, MICP in conjunction with related geochemical tests completed the dynamic characterization of shale pores and concluded the influencing factors of pore development, established an evolution model of shale pore, they considered that the pore evolution of shale was mainly affected by the hydrocarbon generation of organic matter (OM) and the transformation of clay minerals (Wang and Guo, 2019). Peng et al. simulated the hydrocarbon generation process of shale by thermal simulation experiment, and determined the limit of R_o value in the favorable and target areas of shale gas exploration (Peng et al., 2019). Regarding the heterogeneity of pore structure, previous studies believed that the fractal dimension of shale pore structure is negatively related to the pore size, the smaller the pore size, the more complex the pore structure and the worse the connectivity (Yang et al., 2014; Bu et al., 2015; Wang et al., 2015).

Through previous studies, it can be seen that they mainly focus on the division of diagenesis stages, the qualitative analyze in pore structure during thermal evolution, and the establishment of pore evolution models. Quantitative response of shale (especially continental shale) pore structure and its heterogeneity to the hydrocarbon generation (stages and products) is still puzzling and need systematic research. In this study, continental shale of the Ordos Basin was collected to quantitatively discuss the evolution characteristics of pores and their heterogeneity in different hydrocarbon generation stages using thermal simulation experiment, MICP, N_2 and CO_2 adsorption experiments combined with fractal theory. The work clarifies the characteristics and evolution of micropore, mesopore and macropore in the oil and gas window quantitatively, and identifies the variation of heterogeneity of shale during thermal evolution innovatively, which could enhance the understanding of shale pore and provide reference for the research of shale high-quality reservoir.

2. Samples and experiments

2.1. Geological setting and sample

The shale sample in this study was collected from Yanchang Formation of Z284 well in the Yishan slope of the Ordos Basin (Fig. 1). Specific information of sample is shown in Table 1. The Ordos Basin is a multi-cycle sedimentary craton basin in the western North China platform with huge potential of oil and gas resources (Wang et al., 2011; Yang and Deng, 2013; Guo et al., 2018). According to the current tectonic characteristics, the Ordos Basin can be divided into six secondary structural units including the Yimeng uplift, the western marginal thrust belt, the Tianhuan depression, the Yishan slope, the Jinxi fold belt, and the Weibei uplift. The strata in this basin are widely distributed, and all generations of strata have developed to varying degrees. Among them, the Yanchang Formation of Upper Triassic developed a set of river-delta-lake terrigenous clastic sedimentary systems with a total thickness of about 1000–1300 m, the organic-rich shale in it is one of the most important source rock of the Ordos Basin (Wu et al., 2004; Fu et al., 2019).

2.2. Methods

2.2.1. Thermal simulation experiment

Thermal simulation experiment was conducted on the equipment produced by the SGE company. Before the experiment, the

Table 1
Information of core sample Z284. Including the sample depth, Formation, total organic carbon (TOC) content, kerogen type and R_o.

Sample ID	Depth, m	Formation	TOC, wt.%	Kerogen type	R_o, %
Z284	1595.1	Yanchang	1.32	III	0.81

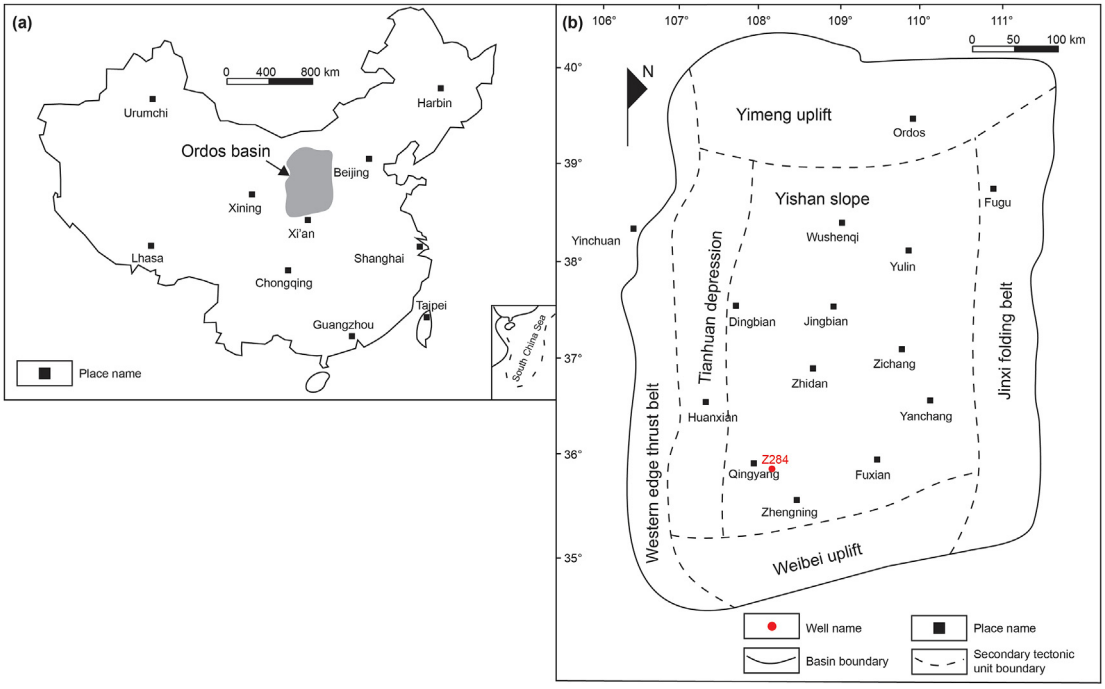

Fig. 1. Geological map of the Ordos Basin and the location of sampling sites.

dried shale sample was separated into 11 fractions. One of them was used for the testing of basic geochemical parameters, including TOC, kerogen type and R_o, and the remaining ten parts were used for thermal simulation experiments. Each remaining sample was then divided into cubes with a length of 1 cm and put in a closed gold tube, heated from room temperature to the preset temperature at a heating rate of 20 °C/h under the constant pressure of 50 MPa. The target temperature was set within a range of 200–650 °C at intervals of 50 °C. To ensure the full progress of experiment, the temperature was kept constant for 2 h after reaching each preset temperature point during thermal simulation experiment. Finally, the gold tubes obtained at different pyrolysis temperatures were placed in a vacuum system after cooling to room temperature. $C_{1\text{-}5}$ hydrocarbons and $C_{6\text{-}14}$ hydrocarbons were measured by the Agilent 6890N gas chromatograph (GC) instrument, while C_{14+} hydrocarbons were extracted by the dichloromethane (CH_2Cl_2), and then the amount of gas hydrocarbon ($C_{1\text{-}5}$) and liquid hydrocarbon ($C_{6\text{-}14}$, C_{14+}) were calculated.

2.2.2. Organic geochemistry

The TOC test of original shale sample was completed on a Leco CS230 carbon/sulfur analyzer. We crushed the sample to 200 mesh first, and then treated with 5% hydrochloric acid to remove the inorganic carbon. Finally, the sample was cleaned with distilled water and dried.

The thermal maturity can be characterized by R_o which refers to the percentage of the reflected light intensity of the vitrinite cut surface and the intensity of the normal incident light at a wavelength of 546 ± 5 nm (green light). The experimental principle is to convert the reflected light intensity into current intensity through a photomultiplier tube, then compare it with the current intensity generated by a standard sample (Yao and Li, 2013; Li et al., 2015; Mathia et al., 2016). The measurement was performed on an MPVSP micro-photometer.

2.2.3. Mineral composition analysis

The mineral composition of shale sample can be obtained by X-ray diffraction (XRD) experiment. XRD of shale powder (crushed to 200–300 mesh) was completed by D8 DISCOVER X-ray diffractometer. The relative mineral percentages were calculated semi-quantitatively by the area under the major peaks curve of each mineral.

2.2.4. MICP

MICP was used to obtain information of macropores, it was performed on an Auto pore 9500 automatic mercury injection instrument. Shale samples were prepared in cylinders with the diameter of 3–10 mm and dried at 110 °C for 24 h. Then we measured the mercury injection and withdrawal quantity under different pressures. Finally, The PV and SSA were obtained by the Washburn equation and Young-Dupré equation respectively (Drummond and Israelachvili, 2002; Brunauer et al., 1938).

2.2.5. Low-pressure CO_2/N_2 adsorption

Low-pressure N_2 adsorption experiment was used to obtain information of mesopores, it was carried out by the Quadrasorb SI specific surface analyzer. Samples were grinded to 50 mesh and we completed the degassing by purging the sample with N_2 under heating until the sample mass no longer changed. N_2 as the adsorbent was then used to perform the adsorption test at a temperature of 77.35 K to obtain the nitrogen adsorption-desorption amount under different relative pressures. The SSA of mesopores was obtained according to the Brunauer-Emmett-Teller (BET) equation; the PV and pore size distributions (PSD) of mesopores were determined by Barrett-Joyner-Halenda (BJH) equation (Brunauer et al., 1938; Barrett et al., 1951).

Low-pressure CO_2 adsorption experiment was used to obtain information of micropores, experiment was conducted on a NOVA4200e specific surface area and pore size distribution analyzer. Samples were grinded into a 60-mesh powder first and purged with CO_2 under heating until the sample mass no longer changed to complete the removal of impurities. Then we measured the adsorption-desorption data of CO_2 at different relative pressures of 273.15 K. Finally, Dubinin Radshkevich (D-R) equation was used to calculate the SSA of micropores, and Dubinin-Astakhov (D-A) equation was used to calculate the PV and PSD of micropores (Dubinin and Stoeckli, 1980).

3. Results

3.1. R_o and mineral composition

The results of XRD and R_o measurement are shown in Table 2. As the simulated temperature increases, R_o increases from 0.82% to 3.35%, which represents the evolution of OM from the early mature stage to the over-mature stage. From the perspective of mineral composition, the sample is mainly composed of clay minerals, quartz and feldspar with a small amount of calcite, dolomite and siderite. The clay minerals, quartz and feldspar account for more than 90% of the total. The mineral composition of sample does not change much with the increase of temperature, only siderite disappears completely after 500 °C (Fig. 2). The clay minerals of the sample mainly include chlorite, illite and I/S, the I/S accounts for more than 60% of the total clay minerals (Fig. 3). With the increase of thermal simulation temperature, the content of chlorite gradually decreases, while the illite and I/S vary complexly.

3.2. Hydrocarbon generation during thermal simulation

The result of hydrocarbon generation result during thermal simulation is shown in Table 3. The production of liquid hydrocarbon shows an increase from 0.07 mg/g at R_o of 0.82% to 0.73 mg/g at R_o of 1.59%, and then turns to decrease from 0.73 mg/g at R_o of 1.59% to 0.07 mg/g at R_o of 3.35% indicating that the liquid hydrocarbon begins to crack to produce gaseous hydrocarbon after R_o is greater than 1.59%. The production of gaseous hydrocarbon increases with the increasing R_o.

Fig. 4 gives an overview of hydrocarbon production to R_o. The production of liquid hydrocarbon is greater than that of gaseous hydrocarbon when R_o is less than 1.59%. The production of gaseous hydrocarbon exceeds that of liquid hydrocarbon after R_o is greater than 1.59%. So we define the stage of R_o<1.59% as the oil window and R_o>1.59% as gas window in this study.

3.3. Micropore characteristics

Fig. 5 shows the adsorption isotherms of CO_2. The adsorption capacity of sample decreases first and then increases with the increasing R_o. The largest adsorption capacity of sample is observed at R_o of 0.82%, and the least one at R_o of 1.12%. This trend is consistent with that of PV and SSA of micropore (Tables 4 and 5), indicating that the development of micropore doesn't follow a simple linear relationship with the increase of R_o.

The PSD of micropore present a bimodal feature, micropore is mainly developed in the pore width intervals of 0.4–0.65 nm and 0.75–0.9 nm and the former is dominating. The PSD of micropore changes with the increasing R_o, micropore significantly reduce and the one above 0.7 nm gradually disappears with the increase of R_o from 0.82% to 1.59%, bimodal distribution becomes unimodal. Then as R_o increases from 1.59% to 3.35%, micropores increase and the

Table 2
Vitrinite reflectance values and mineral compositions of the shale sample obtained from different thermal simulation temperatures.

Temperature, °C	R_o, %	The proportions of mineral composition, %						The proportions of clay composition, %		
		Quartz	Clay	Feldspar	Calcite	Dolomite	Siderite	Chlorite	Illite	I/S
200	0.82	35	46	11	1	6	1	15	23	62
250	0.85	33	45	14	1	6	1	15	21	64
300	1.03	38	41	13	1	6	1	13	24	63
350	1.12	38	43	10	1	7	1	14	26	60
400	1.26	34	42	14	1	8	1	15	27	58
450	1.59	39	40	13	1	6	1	13	24	63
500	1.98	38	39	14	2	7		8	25	67
550	2.32	37	44	12	1	6		5	24	71
600	2.76	40	44	11	1	4		3	30	67
650	3.35	34	46	13	3	4		2	27	71

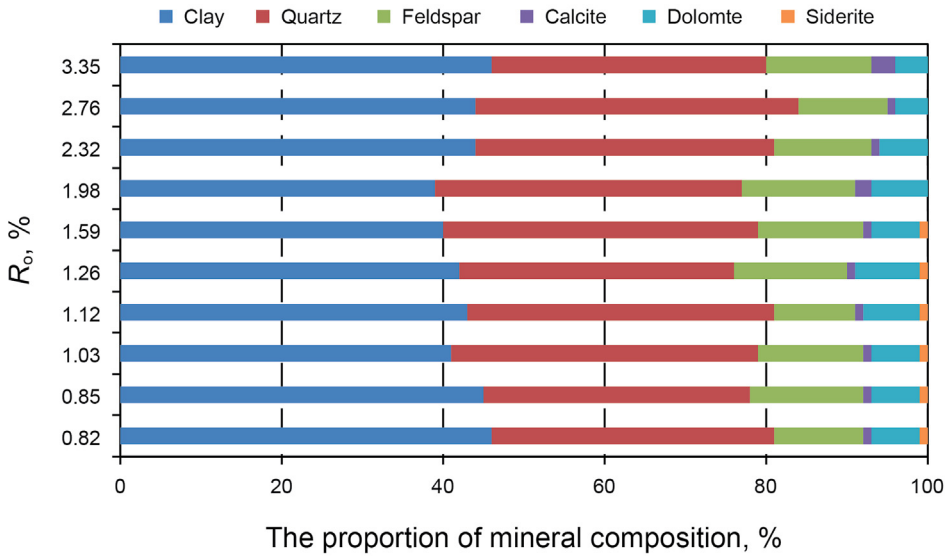

Fig. 2. Variation of mineral composition with R_o.

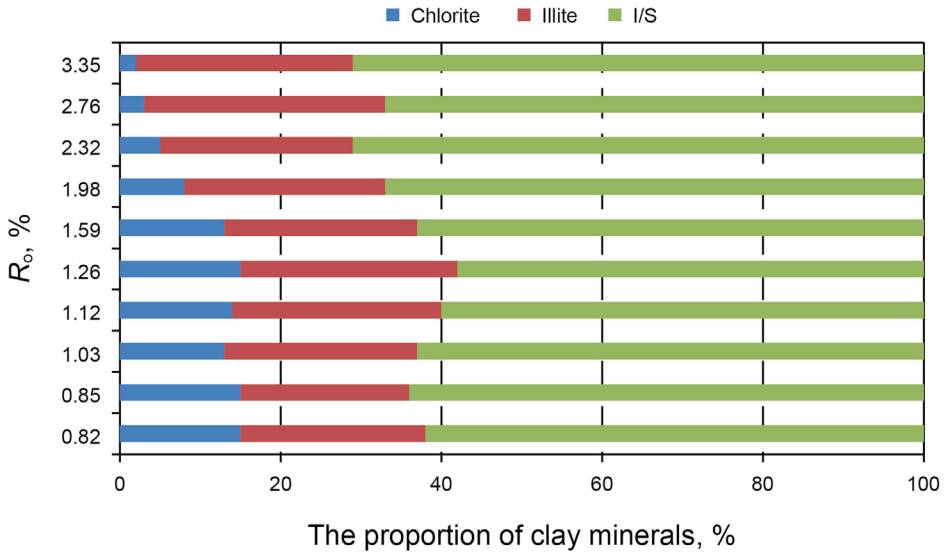

Fig. 3. Variation of clay mineral composition with R_o.

Table 3
Results of hydrocarbon generation of the shale sample during thermal simulation experiment.

R_o, %	Gaseous hydrocarbon production, mg/g	Liquid hydrocarbon production, mg/g	Total hydrocarbon production, mg/g
0.82	0	0.07	0.07
0.85	0	0.1	0.1
1.03	0	0.15	0.15
1.12	0.06	0.24	0.3
1.26	0.2	0.42	0.62
1.59	0.7	0.73	1.43
1.98	1.51	0.52	2.03
2.32	2.07	0.4	2.47
2.76	2.22	0.22	2.44
3.35	2.63	0.07	2.7

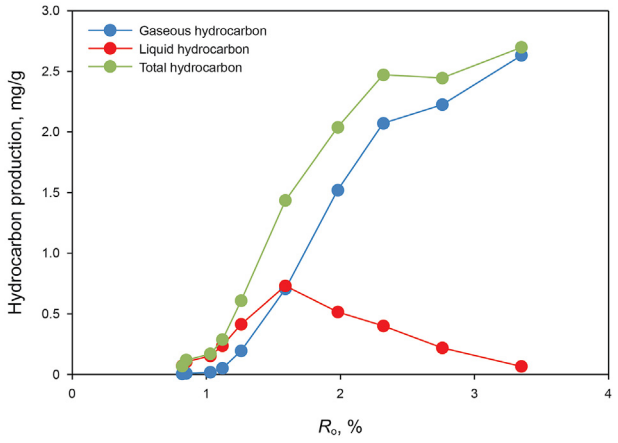

Fig. 4. The relationship between hydrocarbon production and R_o of the shale sample.

micropores of 0.75–0.9 nm appear again, the bimodal characteristics reconstructs (Fig. 6).

3.4. Mesopore characteristics

Mesoporous characterization is completed by N_2 adsorption-desorption isotherm. The variation of N_2 adsorption capacity is different from that of CO_2 adsorption (Fig. 7). The highest adsorption amount is observed at R_o of 3.35%. During the entire thermal evolution process, the adsorption amount shows a trend of first decreasing and then increasing, the minimum adsorption amount appears at the R_o of 1.59% which is also the smallest point of mesopore volume and SSA revealing that the adsorption performance of mesopore is in good agreement with the evolution process of its PV and SSA.

The N_2 adsorption-desorption isotherm of sample belongs to type IV in the IUPAC classification. It is characterized by an obvious hysteresis loop that is used to identify the pore shape. The shape of hysteresis loop in this study is close to type H3 representing the slit-shaped pores created by the accumulation of plate-like particles (Fig. 7). The pore shape of shale sample remains unchanged during the entire thermal evolution process. It indicates that the shape of shale pores has little relationship with the thermal evolution of OM.

Fig. 8 shows the PSD of mesopore, the development of mesopore is better than that of micropore. The mesopore decreases with the increase of R_o from 0.82% to 1.59%, especially, when R_o is between 1.59 and 2.32%, the mesopore above 40 nm disappears. When R_o is greater than 2.32%, mesopore with large pore diameters above 40 nm reappears, the mesopore volume of this part increases compared with the starting point. Finally, the mesopore volume reaches the maximum when R_o = 3.35%. On the whole, the mesopore increases from low-maturity to over-maturity, indicating that

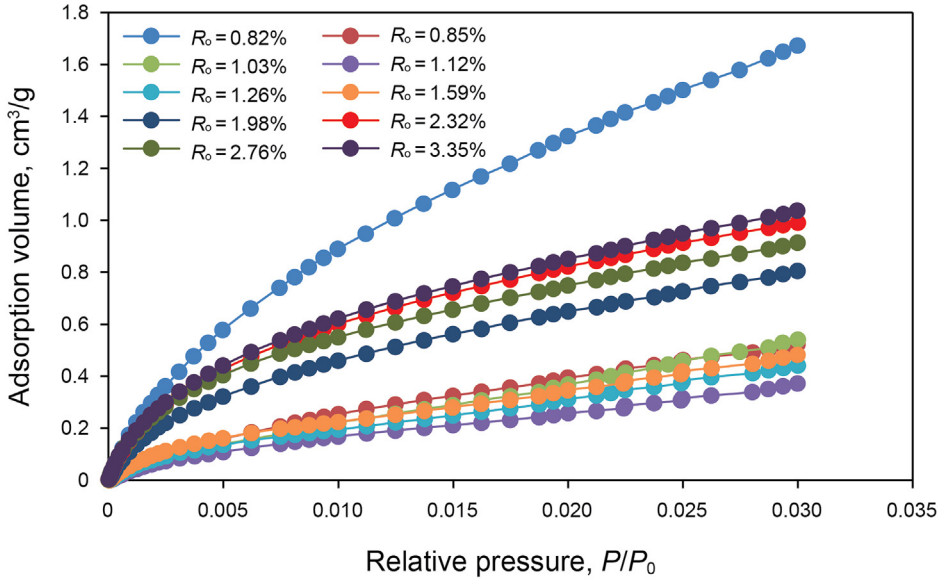

Fig. 5. Low–pressure CO2 adsorption isotherms of the shale sample.

Table 4
The whole-aperture pore volume distribution characteristics of the shale sample.

Thermal simulation temperature, °C	R_o, %	Pore volume, cm^3/g				The proportions of pore volume, %		
		Micropore	Mesopore	Macropore	Total pore	Micropore	Mesopore	Macropore
200	0.82	0.00186	0.00504	0.0164	0.0233	7.98	21.63	70.39
250	0.85	0.00046	0.00417	0.0108	0.01543	2.98	27.03	69.99
300	1.03	0.00029	0.00464	0.0159	0.02083	1.39	22.28	76.33
350	1.12	0.00026	0.00428	0.0118	0.01634	1.59	26.19	72.22
400	1.26	0.00029	0.00438	0.0093	0.01397	2.08	31.35	66.57
450	1.59	0.00036	0.00285	0.005	0.00821	4.38	34.71	60.90
500	1.98	0.00098	0.00479	0.0044	0.01017	9.64	47.10	43.26
550	2.32	0.00131	0.00528	0.011	0.01659	7.90	25.80	66.31
600	2.76	0.00115	0.00839	0.0067	0.01624	7.08	51.66	41.26
650	3.35	0.00133	0.00915	0.021	0.03148	4.22	29.07	66.71
Average		0.000829	0.00519	0.01123	0.017249	4.81	30.09	65.11

Table 5
The whole-aperture specific surface areas of the shale sample.

Thermal simulation temperature, °C	R_o, %	Surface areas, m^2/g				The proportions of surface areas, %		
		Micropore	Mesopore	Macropore	Total pore	Micropore	Mesopore	Macropore
200	0.82	6.123	2.080	0.027	8.230	74.396	25.276	0.328
250	0.85	1.516	1.086	0.002	2.604	58.219	41.704	0.077
300	1.03	1.019	1.464	0.016	2.499	40.770	58.589	0.640
350	1.12	0.936	1.167	0.027	2.130	43.936	54.797	1.267
400	1.26	1.071	1.012	0.044	2.127	50.342	47.590	2.068
450	1.59	1.342	0.716	0.001	2.059	65.183	34.769	0.049
500	1.98	3.376	1.515	0.001	4.892	69.018	30.962	0.020
550	2.32	4.535	0.968	0.087	5.590	81.121	17.323	1.556
600	2.76	4.106	2.311	0.084	6.501	63.157	35.551	1.292
650	3.35	4.623	2.249	0.06	6.932	66.691	32.443	0.866
Average		2.8647	1.457	0.0349	4.357	65.756	33.443	0.801

the thermal evolution process of OM is conducive to the development of mesopore. In particular, mesopores with large pore diameters develop in the over-mature stage when R_o is greater than 2%.

3.5. Macropore characteristics

MICP is used to the quantitative characterization of macropore. Result shows that macropore provides a huge part of the PV, but its contribution to the SSA is small and can be ignored (Tables 4 and 5). The macropore shows a decrease with the increasing R_o before 1.98%, and then a increase with further increasing R_o from 1.98% to 3.35%. The macropore PSD shows that it is mainly provided by the pores between 50-250 μm and 300–400 μm, and the former one is dominant. The macropore of 50–250 μm gradually decreases with the increase of R_o from 0.82% to 2.76% and increases from 2.76% to 3.35%. The macropore of 300–400 μm increases with the increasing R_o, and reaches the maximum at R_o of 3.35% (Fig. 9).

3.6. Fractal dimension

Fractal dimension is an important concept in fractal geometry, it was first proposed by French mathematician Mandelbrot to characterize the complexity and irregularity of the morphological structure of objects. It was later introduced into geosciences and widely used in the heterogeneity analysis of rock. In this study, N_2 adsorption and MICP data were used to calculate the fractal dimensions of shale pores at different temperature points in the thermal simulation process.

N_2 adsorption data is used to calculate the fractal dimension based on the Frenkel-Halsey-Hill (FHH) model, the calculation formula is as follows:

$$\ln(V) = K\left(\ln\left(\frac{p_0}{p}\right)\right) + C \quad (1)$$

where V represents the gas adsorption capacity at equilibrium pressure P, P_0 is saturation pressure of the gas, C is a constant, K is the slope of the straight line. If the shale has fractal characteristics, linear relationship exists between ln$V$ and ln (P_0/P), and the slope K can be obtained by fitting curve. The fractal dimension D depends on the value of K. When the adsorption mechanism of sample is capillary condensation, $D = K+3$. When the adsorption mechanism is van der Waals force, $D = 3K+3$ (Pfeifer et al., 1989; Faulon et al., 1994; Gauden et al., 2001; Xie et al., 2014). In actual research, Yao et al. further divided the fractal dimension into D_1 and D_2 according to different pressure intervals ($P/P_0 < 0.5$ and $0.5 < P/P_0 < 1$), where D_1 represents the fractal dimension of pore surface characterizing the roughness of small pores; D_2 represents the fractal dimension of pore structure, which is used to characterize the complexity of large pores. Both of them are usually between 2 and 3, and the closer to 3, the rougher the pore surface and the more complex the structure (Yao et al., 2008). In this experiment, the N_2 adsorption and desorption branches does not overlap, indicating that capillary condensation occurred, so $D = K+3$ is used to calculate the fractal dimension.

The fitting result shows that ln$V$ and ln (P_0/P) have segmental characteristics in the intervals of $P/P_0 < 0.5$ and $0.5 < P/P_0 < 1$ (Fig. 10). The fitting degree in each interval is high, and the correlation coefficient are both greater than 0.9. According to the slope of each curve, the fractal dimension D_1 and D_2 are obtained according to formula of $D = K+3$, both of them are between 2 and 3, which in line with fractal theory (Table 6).

The calculation formula for calculating the fractal dimension of MICP is as follows:

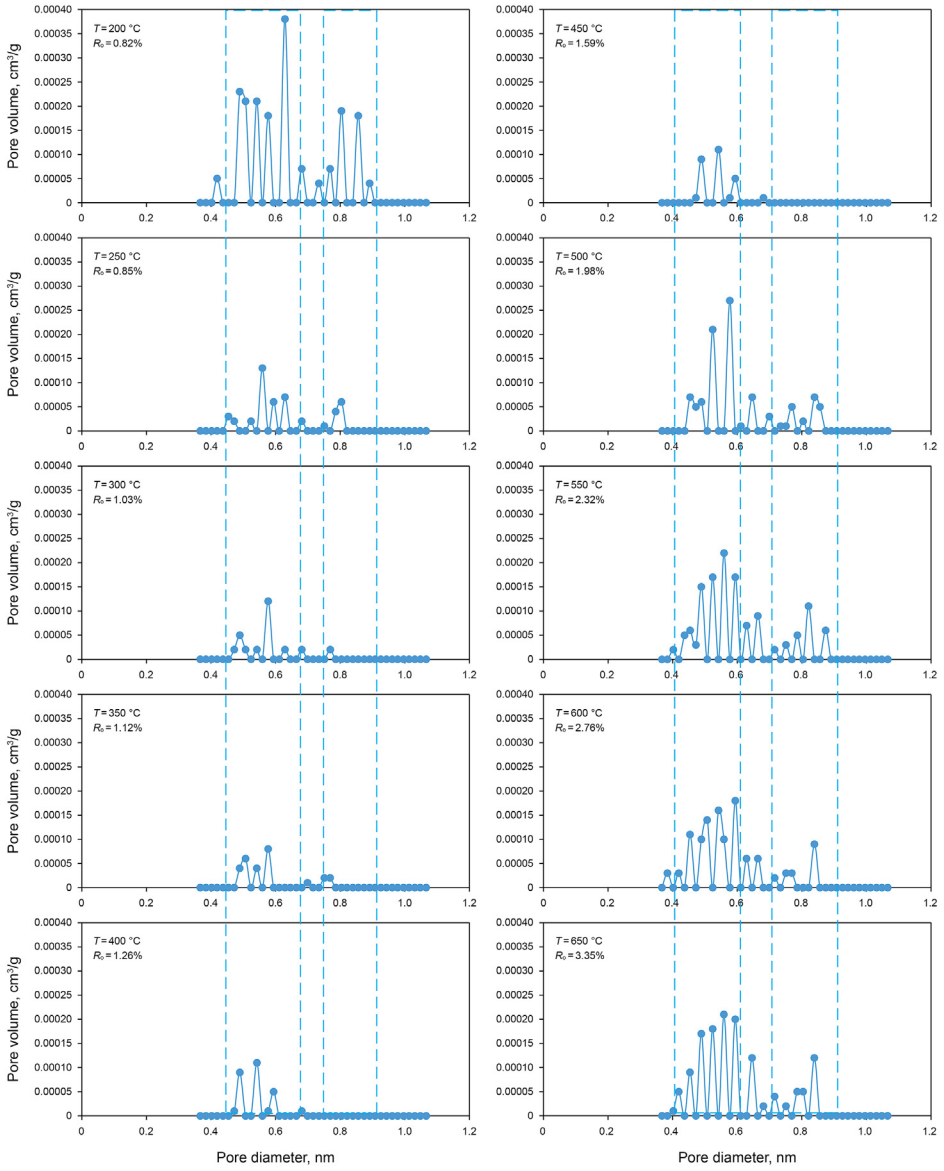

Fig. 6. PSD of micropore derived from CO_2 adsorption.

$$\lg(1 - S_{Hg}) = (D - 3)\lg P_c + (3 - D)\lg P_{min} \quad (2)$$

where S_{Hg} represents the cumulative mercury saturation; P_c stands for capillary pressure; P_{min} represents the capillary pressure corresponding to the maximum aperture; D is the fractal dimension. The fractal dimension can be obtained by the slope of the intersection of $\lg(1\text{-}S_{Hg})$ and $\lg P_c$. The fitting results show that the MICP fractal also presents segmental characteristics, and the correlation within each segment is good (Fig. 11). The fractal dimensions D_1 and D_2 of the two fitting curves are also between 2 and 3 which conform to the fractal theory too (Table 7).

4. Discussion

4.1. Quantitative analysis of shale pores during hydrocarbon generation

Hydrocarbon generation of organic-rich shale is a complex chemical process whose products can be divided into liquid hydrocarbon and gaseous hydrocarbon according to phases (Dembicki et al., 1983; Curtis et al., 2012; Furmann et al., 2013). The hydrocarbon generation of sample is divided into two stages including oil window and gas window according to the relationship between hydrocarbon products and R_o. The quantitative evolution characteristics of pores in these two stages will be discussed below. It is worth mentioning that the sample in this study has a high maturity, it can not characterize the lower evolution stage smaller than 0.81% indeed, but the research of Kuila and Prasad showed that as shale has not yet entered the "oil window", the transformation of clay minerals are not obvious, the main reason for the reduction in the SSA and PV in this stage is compaction, so the high maturity of our sample may not influence the discussion of shale pore evolution during hydrocarbon generation.

4.1.1. Micropore

The PV and SSA of micropore have the same evolution trend, both of them decrease first and then increase with the increase of R_o (Fig. 12).

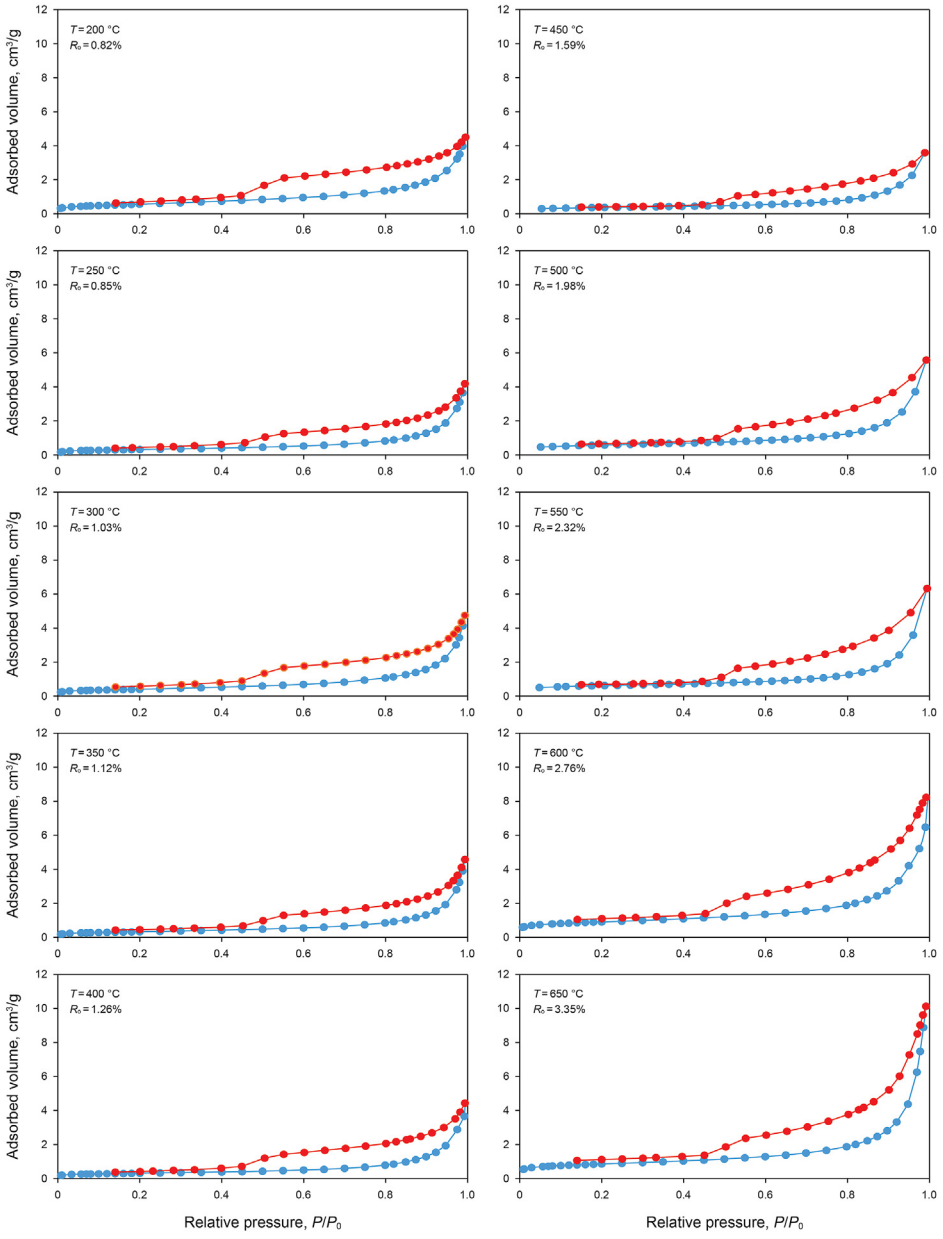

Fig. 7. N_2 adsorption-desorption isotherm of the shale sample.

In the oil window, The PV and SSA of micropore decrease first and then slightly increase with the increase of R_o, but it is still a decreasing process on the whole. The PV of micropore decreases from 0.00186 cm^3/g at R_o of 0.82% to 0.00036 cm^3/g at R_o of 1.59%, with a total reduction of 80.65%; the SSA decreases from 6.123 m^2/g at R_o of 0.82% to 1.342 m^2/g at R_o of 1.59%, with a total reduction of 78.08%. Previous studies considered that asphaltene and liquid hydrocarbon produced by the thermal degradation of OM will block the pores leading to a decrease in pore volume (Mastalerzet al., 2013; Valenza et al., 2013; Lin et al., 2014; Pommer and Milliken, 2015). In the early stage of oil window, a large amount of liquid hydrocarbon is produced and quickly occupies the pores, which greatly reduces the pore volume (Fig. 13a). With the further evolution, the dissolution of organic acids and the transformation of clay minerals from disorder to order promote the slightly increase of PV (Zhao and He, 2012), the good correlation between micropore volume and clay content proved this conclusion (Fig. 14a). So the change of micropore volume in the oil window is mainly controlled by the combined effect of asphaltene filling and clay mineral transformation, and the former one is dominant.

In the gas window, the PV and SSA of micropore increase with the increasing R_o overall. The PV of micropore increases from 0.00036 cm^3/g at R_o of 1.59% to 0.00133 cm^3/g at R_o of 3.35%, which increases 2.69 times; the SSA increases from 1.342 m^2/g at R_o of 1.59% to 4.632 m^2/g at R_o of 3.35%, with a total increase of 2.45 times. The development of micropore in this stage has a good positive correlation with gaseous hydrocarbon production, and the correlation coefficient can reach 0.8991 (Fig. 13b), indicating that the gas window is conducive to the development of micropore. In this process, the consumption of OM and the cracking of liquid hydrocarbons will release a lot of space, resulting in an increase in pore volume (Loucks et al., 2009; Curtis et al., 2012a, 2012b; Modica and Lapierre, 2012; Mastalerz et al., 2013; Milliken et al., 2013; Pommer and Milliken, 2015). In addition, there is a good positive

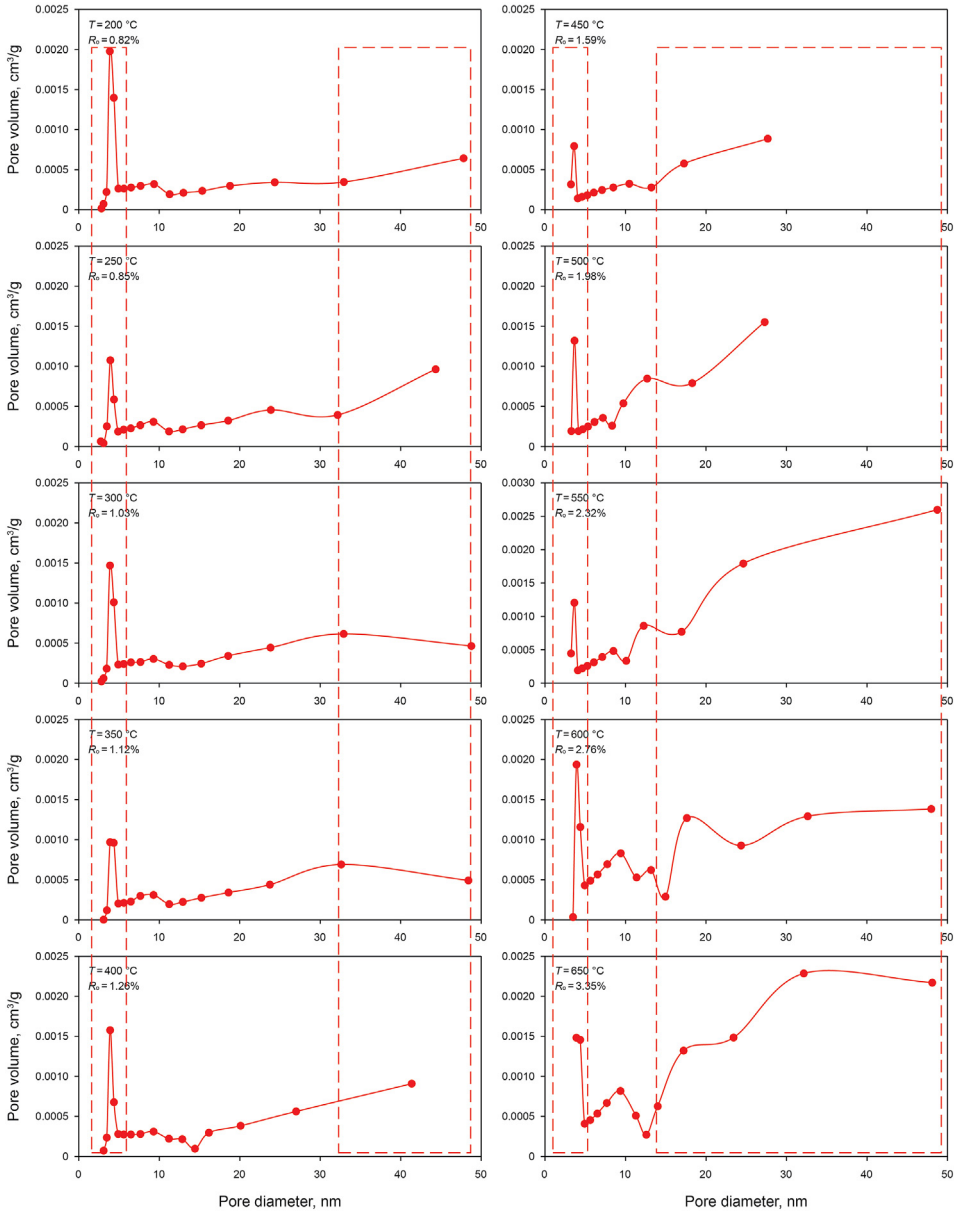

Fig. 8. PSD of mesopore derived from N_2 adsorption.

correlation between the micropore volume and the relative content of I/S, the correlation coefficient is 0.8857 (Fig. 14b), it is related to the large number of interlayer pores of I/S, which provides a large amount of pore space. It can be concluded that the cracking of liquid hydrocarbons and the conversion of clay minerals to I/S in the gas window work together to promote the development of micropore in this stage.

4.1.2. Mesopore

The PV and SSA of mesopore also show the same trend with that of micropore (Fig. 15). In the oil window, both of them decrease with the increase of R_o overall, although there are some fluctuate slightly. The PV of mesopore decreases from 0.00504 cm^3/g at R_o of 0.82% to 0.00285 cm^3/g at R_o of 1.59%, with a total reduction of 43.45%; the SSA decreases from 2.080 m^2/g at R_o of 0.82% to 0.716 m^2/g at R_o of 1.59%, with a total reduction of 65.6%. It can be seen from the relationship between liquid hydrocarbon production and mesopore volume at this stage that there is a linear negative correlation between them, with a correlation coefficient of 0.7592 (Fig. 13c), but the mesopore have little relationship with clay minerals (Fig. 14c), indicating that the mesopore is greatly affected by the production of liquid hydrocarbons, namely the liquid hydrocarbons and asphaltenes generated by the degradation of OM block the mesopore (Loucks et al., 2009; Modica and Lapierre, 2012; Mastalerz et al., 2013; Pommer and Milliken, 2015).

In the gas window, the PV and SSA of mesopore continue to increase with the increasing R_o. The PV of mesopore increases from 0.00285 cm^3/g at R_o of 1.59% to 0.00915 cm^3/g at R_o of 3.35%, which increases 2.21 times; the SSA increases from 0.716 m^2/g at R_o of 1.59% to 2.249 m^2/g at R_o of 3.35%, with a total increase of 2.14 times. The development of mesopore in this stage has a good positive correlation with gaseous hydrocarbon production, the correlation coefficient is 0.8524 (Fig. 13d), showing that the gas generation is also conducive to the development of mesopore. Wang and Guo (2019) hold that the main reason for the development of mesopore in this stage is the dissolution of feldspars and

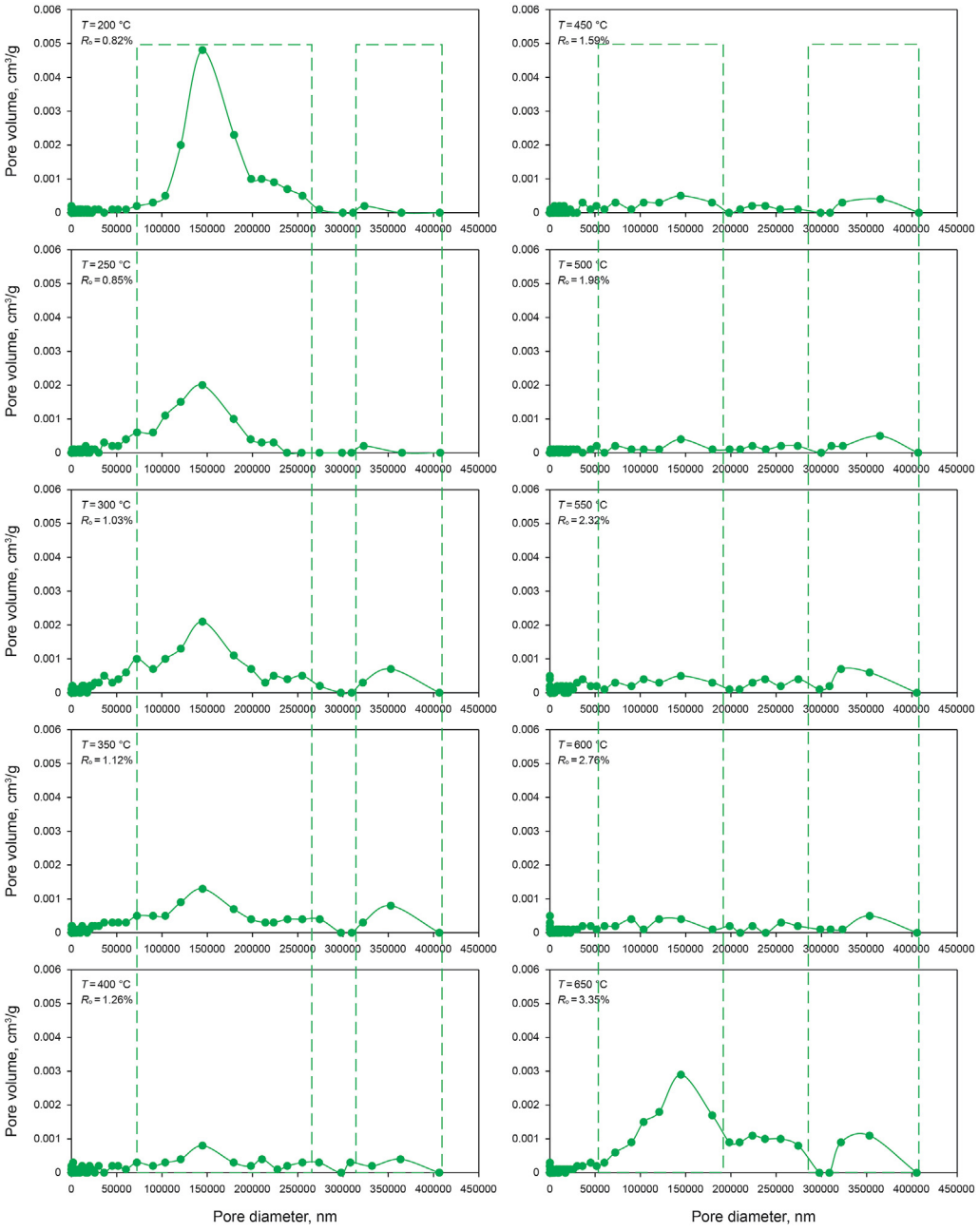

Fig. 9. PSD of macropore derived from MICP.

clay minerals by organic acids originating from hydrocarbon generation and the formation of shrinkage cracks associated with hydrocarbon generation. In addition, the generation of gaseous hydrocarbon originating from kerogen pyrolysis and liquid hydrocarbon cracking can generate high pore pressures in shale which also conducive to the development of mesopore. In our study, there is a good negative correlation between mesopore volume and chlorite content, with a correlation coefficient of 0.8778 (Fig. 14d), indicating that the conversion of chlorite to illite in the gas window also promote the development of mesopore.

4.1.3. Macropore

Since the SSA of macropore is too small compared with micropore and mesopore, the contribution of it to the shale can be negligible, only the evolution of macropore volume is discussed in this paper. The macropore volume decreases first and then increases with the increasing R_o (Fig. 16). In the oil window, The PV of macropore decreases from 0.0164 cm^3/g at R_o of 0.82% to 0.005 cm^3/g at R_o of 1.59%, with a total reduction of 69.51%. There is a negative correlation between macropore volume and liquid hydrocarbon production, and the correlation coefficient is 0.7738 (Fig. 13e), the content of clay mineral shows no correlation with macropore (Fig. 14e). Thus, it can be concluded that the reduction of macropore volume is mainly affected by liquid hydrocarbons, and the reason is speculated to be the same as that of mesopore, which is caused by the blockage of liquid hydrocarbon and asphaltene generated by the degradation of OM (Mastalerz et al., 2013; Milliken et al., 2013; Pommer and Milliken, 2015).

In the gas window, the PV of macropore increases with the increasing R_o, it increases from 0.005 cm^3/g at R_o of 1.59% to

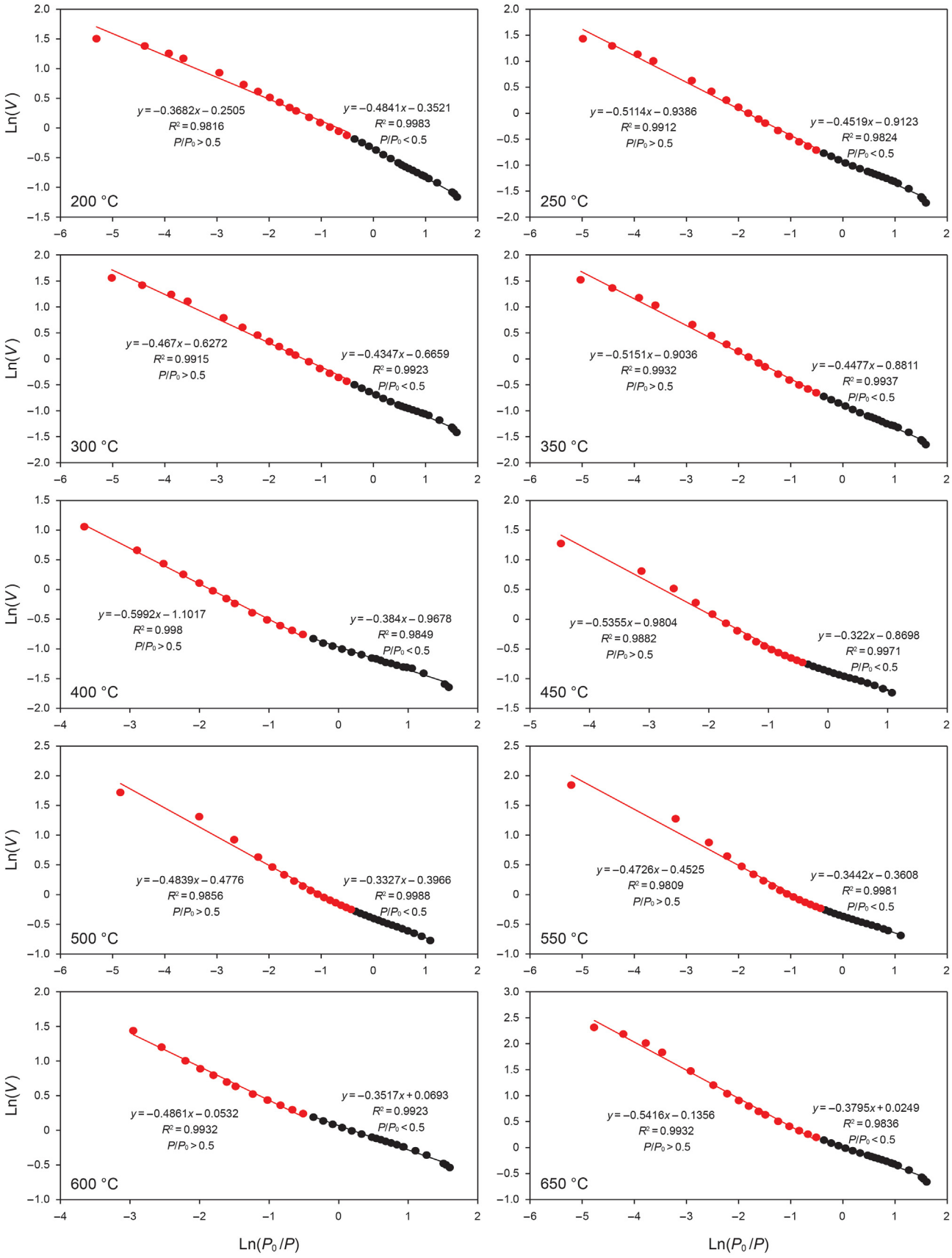

Fig. 10. Double logarithm curves of N_2 adsorption volume and relative pressure.

Table 6
Fractal dimensions calculated by N_2 adsorption data.

Temperature, °C	P/P_0<0.5			P/P_0>0.5		
	Fitting equation	Fitting coefficient	D_1	Fitting equation	Fitting coefficient	D_2
200	$y = -0.3682x - 0.2505$	0.9816	2.6318	$y = -0.4841x - 0.3521$	0.9983	2.5159
250	$y = -0.5114x - 0.9386$	0.9912	2.4886	$y = -0.4519x - 0.9123$	0.9824	2.5481
300	$y = -0.4670x - 0.6272$	0.9915	2.533	$y = -0.4347x - 0.6659$	0.9923	2.5653
350	$y = -0.5151x - 0.9036$	0.9932	2.4849	$y = -0.4477x - 0.8811$	0.9937	2.5523
400	$y = -0.5992x - 1.1017$	0.9980	2.4008	$y = -0.384x - 0.9678$	0.9849	2.6160
450	$y = -0.5355x - 0.9804$	0.9882	2.4645	$y = -0.322x - 0.8698$	0.9971	2.6780
500	$y = -0.4839x - 0.4776$	0.9856	2.5161	$y = -0.3327x - 0.3966$	0.9988	2.6673
550	$y = -0.4726x - 0.4525$	0.9809	2.5274	$y = -0.3442x - 0.3608$	0.9918	2.6558
600	$y = -0.4861x - 0.0532$	0.9932	2.5139	$y = -0.3517x + 0.0693$	0.9923	2.6483
650	$y = -0.5416x - 0.1356$	0.9932	2.4584	$y = -0.3795x + 0.0249$	0.9836	2.6205

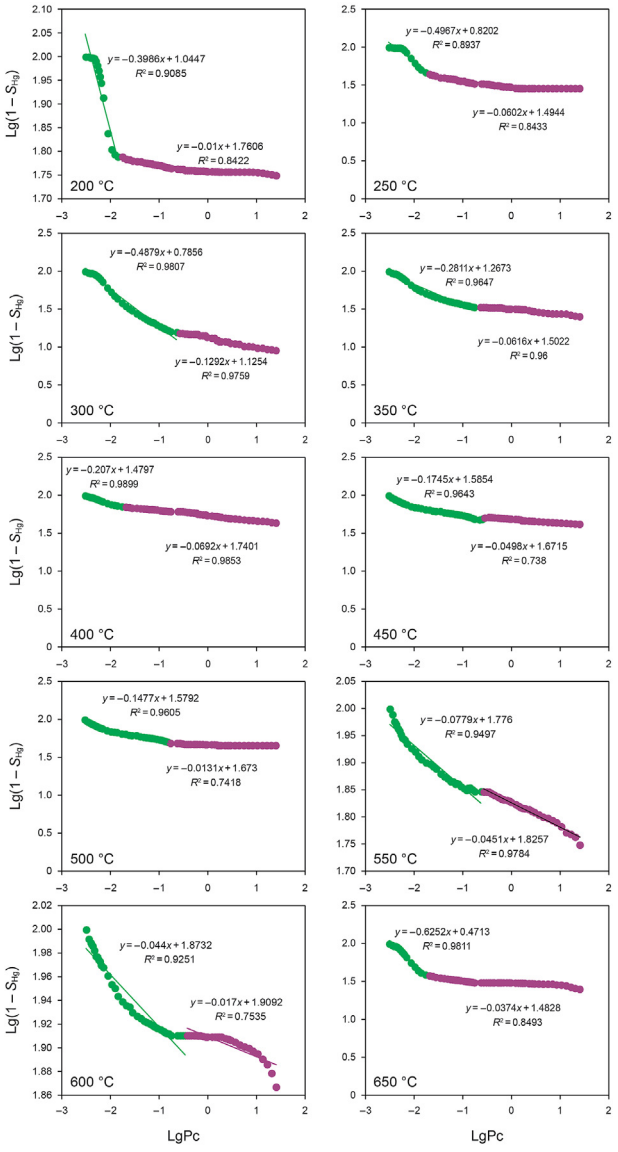

Fig. 11. Double logarithm curves of wetting phase saturation and capillary pressure.

0.021 cm^3/g at R_o of 3.35% with a increases of 3.2 times. The development of macropore in this stage has a certain positive correlation with gaseous hydrocarbon production, but the correlation is not as good as that of mesopore and micropores, the correlation coefficient is only 0.5466 (Fig. 13f), the relative content of I/S shows a good positive correlation with macropore volume, and the correlation coefficient is 0.7208 (Fig. 14f), indicating that the transformation of clay minerals to I/S is a key factor to promote the development of macropore in the gas window. In addition, some scholars believe that the combination and connection of a large number of micropore is also an important factor in the increase of macropore volume at this stage (Chen and Xiao, 2014; Hu et al., 2017).

To sum up, the oil generation stage dominated by liquid hydrocarbons (R_o < 1.59) is not conducive to the development of micropore, mesopore and macropore, the negative effect on micropore is the largest, followed by macropore. In terms of influencing factors, micropore is mainly affected by the transform of clay minerals; while macropore and mesopore are mainly affected by liquid hydrocarbon and asphaltene plugging, the transform of clay minerals is not the main controlling factor. The gas generation stage dominated by gaseous hydrocarbon is conducive to the development of micropore, mesopore and macropore, the development of pores at this stage are mainly controlled by the space releasing of hydrocarbon cracking and the transform of clay minerals to I/S. Therefore, we can initially define R_o>1.59% as a favorable stage for pore development in continental shale.

4.2. Influence of thermal evolution on pore heterogeneity

4.2.1. N_2 adsorption

The fractal dimension D_1 of N_2 adsorption changes complicatedly with the increasing R_o, there is no obvious regular pattern (Fig. 17a). But it has a certain relationship with hydrocarbon production. In the oil window, D_1 decreases first and then increases slightly with the increase of liquid hydrocarbon production (Fig. 18a), indicating that the thermal evolution of OM to generate liquid hydrocarbon reduces the roughness of shale pore surface of small pore. It is inferred that the organic acid generated by the pyrolysis of OM dissolves the pores, which makes the pore surface smooth. When the liquid hydrocarbon production approaching the peak, the output of organic acid gradually decreases, and the evolution of pores plays a leading role, making the pore surface roughness further increase. In the gas window, D_1 shows the same trend as that of oil window, but varies little overall, showing that the intermediate products of the cracking of liquid hydrocarbons affect the roughness of pore surface, but as the cracking ends, this effect gradually disappears (Fig. 18c).

The fractal dimension D_2 increases first and then decreases with the increasing R_o too, the correlation coefficient is 0.8788, showing that the structure heterogeneity of large pore has a good correlation with the thermal evolution process of shale. In the oil window, there is a clear linear positive correlation between the production of liquid hydrocarbon and D_2, the correlation coefficient is 0.95

Table 7
Fractal dimensions calculated by MICP data.

Temperature,°C	Fitting equation	Fitting coefficient	D_1	Fitting equation	Fitting coefficient	D_2
200	$y = -0.3986x+1.0447$	0.9085	2.6014	$y = -0.0100x+1.7606$	0.8422	2.9990
250	$y = -0.4967x+0.8202$	0.8937	2.5033	$y = -0.0602x+1.4944$	0.8433	2.9389
300	$y = -0.4879x+0.7856$	0.9807	2.5121	$y = -0.1292x+1.1254$	0.9759	2.8708
350	$y = -0.2811x+1.2673$	0.9647	2.7189	$y = -0.0616x+1.5022$	0.9600	2.9384
400	$y = -0.2070x+1.4797$	0.9899	2.7930	$y = -0.0692x+1.7401$	0.9853	2.9308
450	$y = -0.1445x+1.5854$	0.9643	2.8555	$y = -0.0106x+1.6715$	0.738	2.9502
500	$y = -0.1477x+1.5792$	0.9605	2.8523	$y = -0.0131x+1.6730$	0.7418	2.9869
550	$y = -0.0779x+1.7760$	0.9497	2.9211	$y = -0.0451x+1.8257$	0.9784	2.9549
600	$y = -0.0440x+1.8732$	0.9251	2.9560	$y = -0.017x+1.9092$	0.7535	2.9830
650	$y = -0.6252x+0.4713$	0.9811	2.3748	$y = -0.0374x+1.4828$	0.8493	2.9626

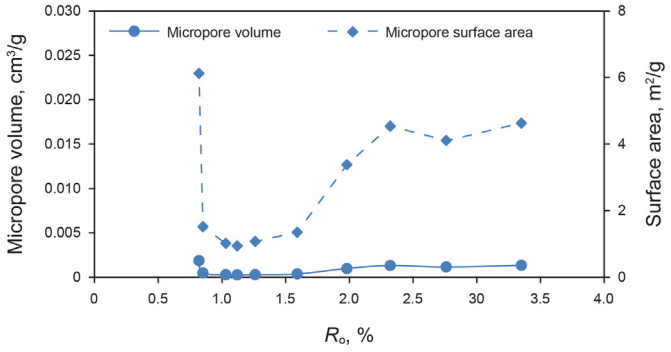

Fig. 12. The development of PV and SSA of micropore with R_o.

(Fig. 18b), indicating that the pore structure of large pore becomes more complex during the process of OM pyrolysis to generate liquid hydrocarbon. The reason may be that the oil generated in this stage is mainly stored in the form of retained oil and filled in pores, a large amount of oil retention leads to the plugging or sealing of connected pores, resulting in the complexity of pore structure. In the gas window, the gaseous hydrocarbon production is linearly negatively correlated with D_2, the correlation coefficient is 0.84 (Fig. 18d). The pore structure heterogeneity of large pore at this stage becomes smaller, it may be caused by the cracking of liquid hydrocarbon releasing the space and channels occupied by it,

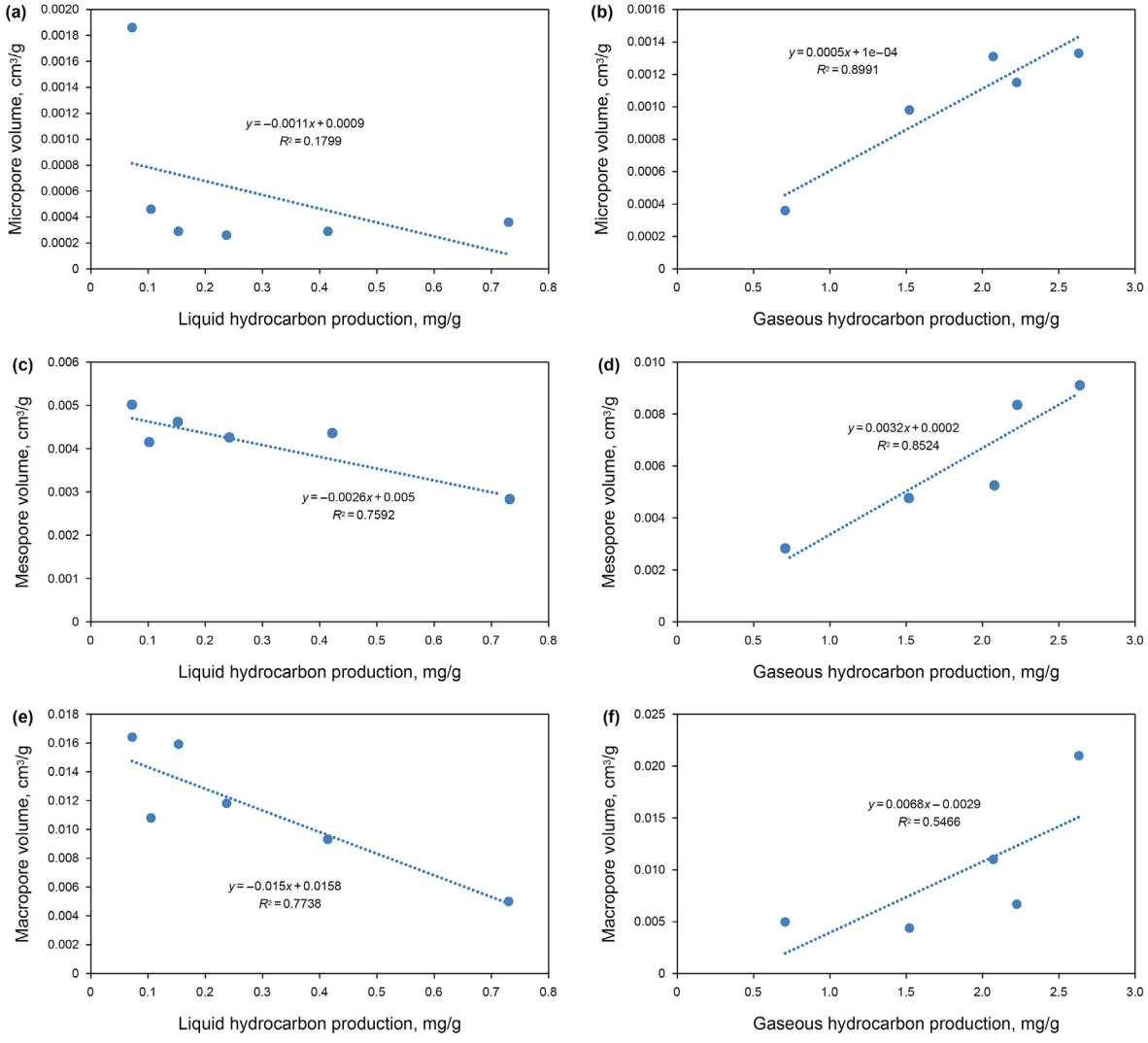

Fig. 13. The relationship between pore development and the production of hydrocarbons.

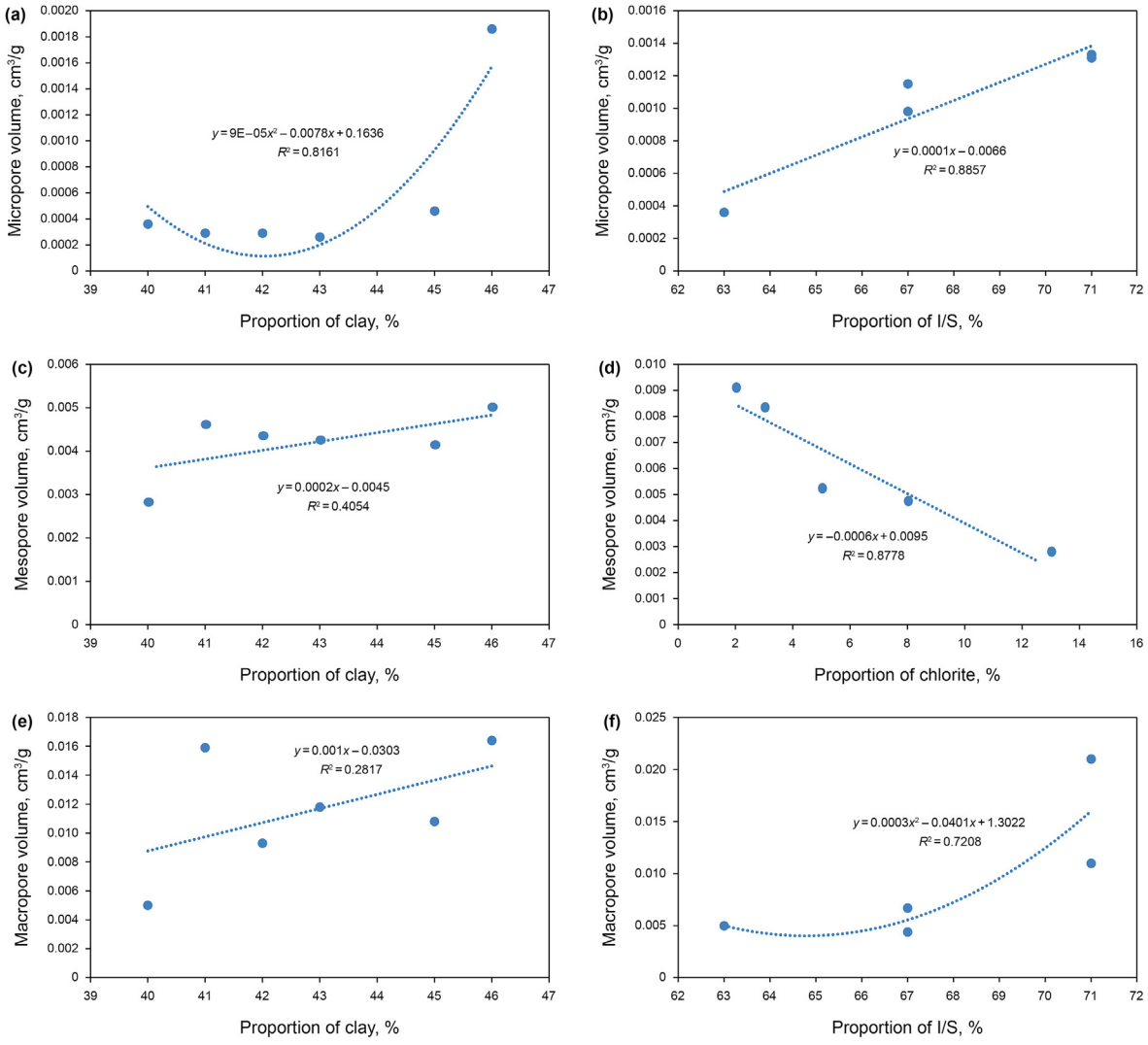

Fig. 14. The relationship between pore development and clay minerals.

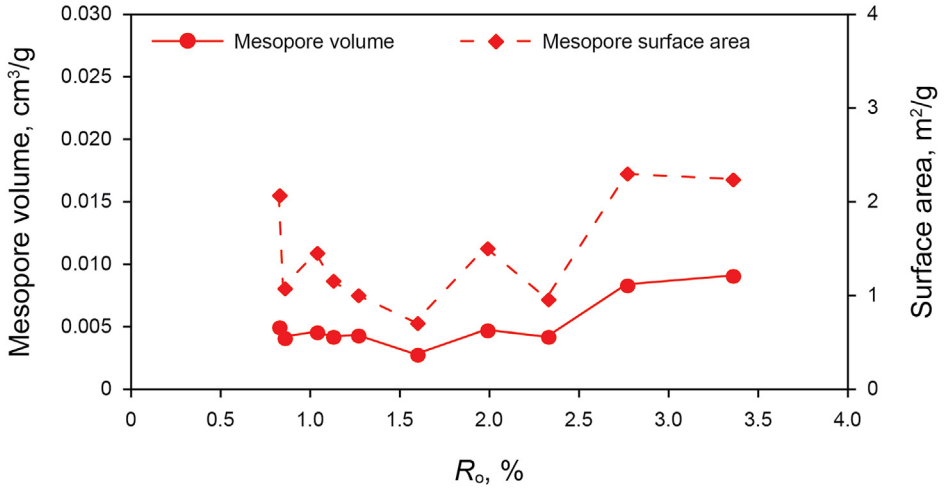

Fig. 15. The development of PV and SSA of mesopore with R_o.

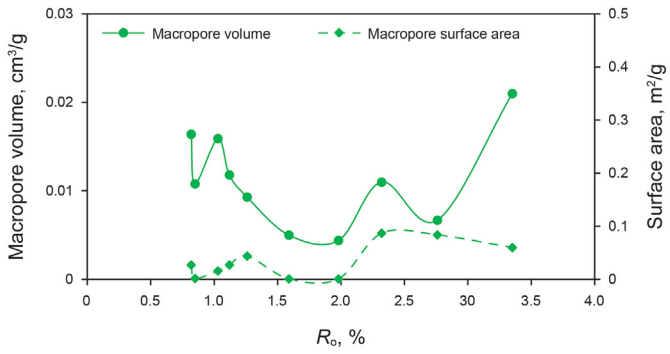

Fig. 16. The development of PV and SSA of macropore with R_o.

which is conducive to the connection of pores.

4.2.2. MICP

The fractal dimension D_1 of MICP shows a trend of first increasing and then decreasing with the increase of R_o (Fig. 19a), indicating that the heterogeneity of small pore first increased and then decreased with the increase of R_o. The fractal dimension D_2 does not change much with R_o (Fig. 19b), indicating that the heterogeneity of large pore is less affected by thermal evolution. Comparing D_1 and D_2, it can be seen that D_2 is larger than D_1 as a whole, indicating that the heterogeneity of large pore is stronger than that of small pore size.

It can be seen from the relationship between thermal evolution hydrocarbon generation products and MICP fractal dimension that

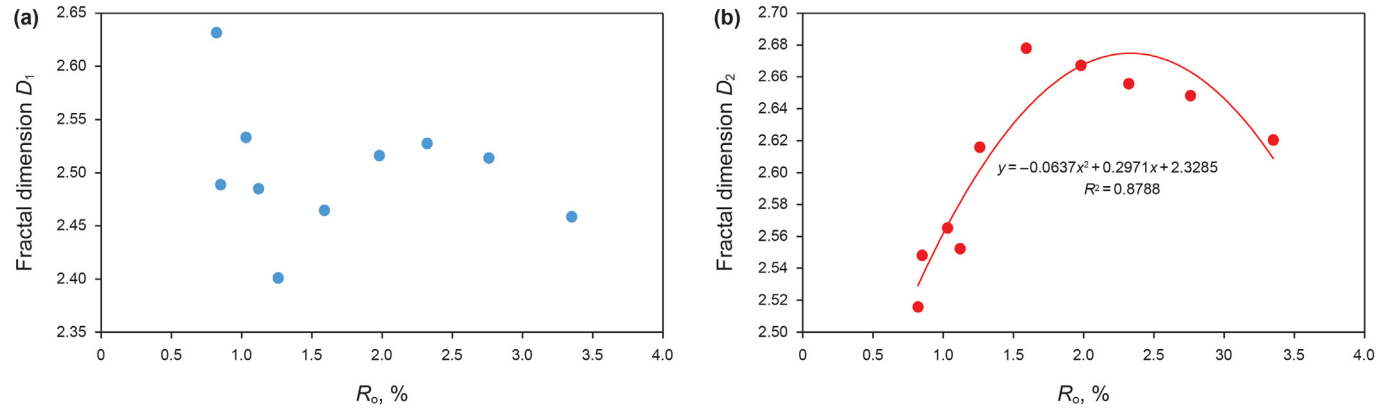

Fig. 17. Relationship between fractal dimension of N_2 adsorption and R_o.

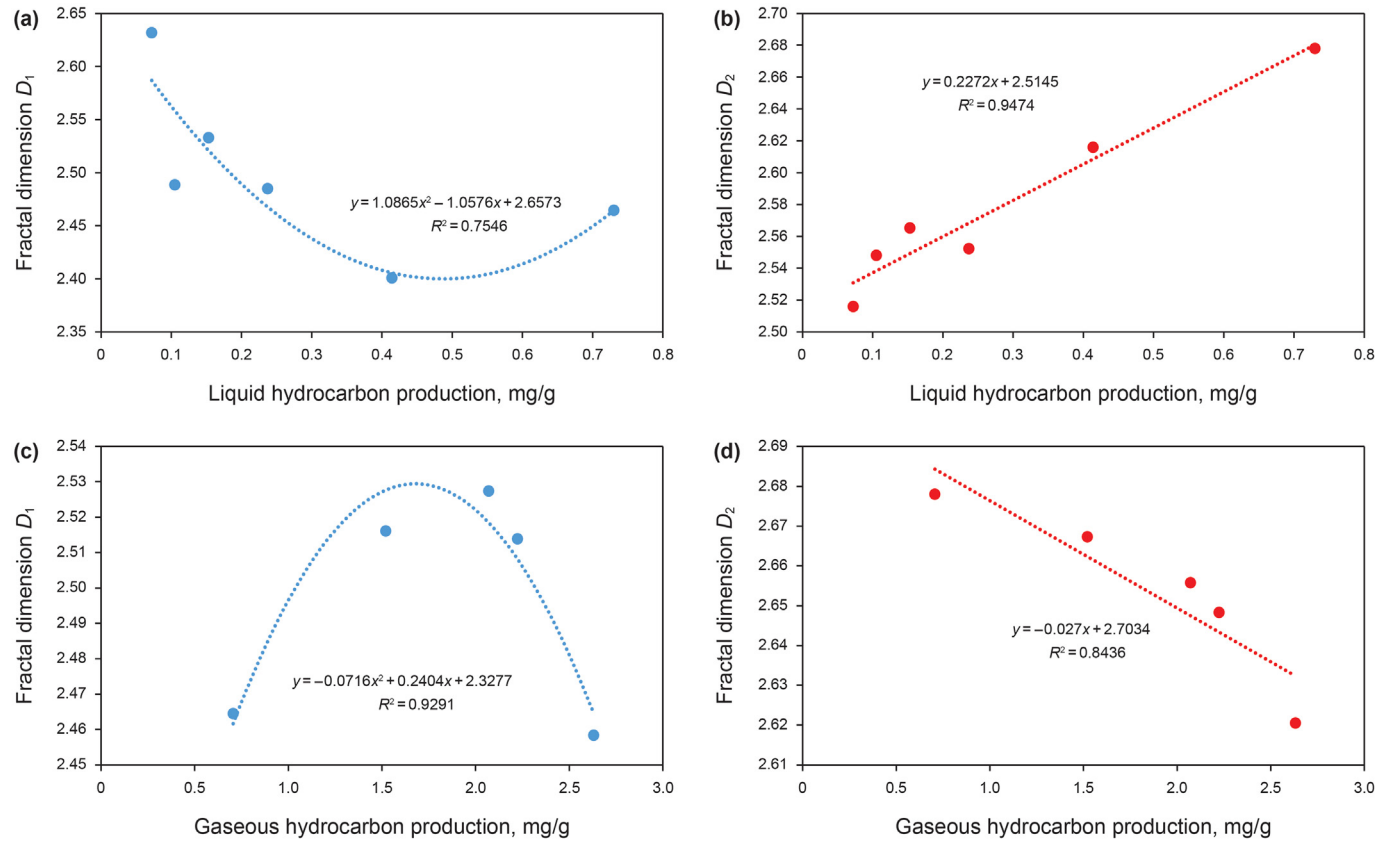

Fig. 18. Relationship between fractal dimension of N_2 adsorption and the hydrocarbon production.

the fractal dimension D_1 increases with the increase of liquid hydrocarbon production (Fig. 20a), indicating that the stage of liquid hydrocarbon generation will enhance the heterogeneity of small pores. The fractal dimension D_2 remains basically constant during the liquid hydrocarbon production stage (Fig. 20b), indicating that liquid hydrocarbon generation has little effect on the heterogeneity of large pores. In the gas generation stage, D_1 first increases and then decreases with the increase of gaseous hydrocarbon production (Fig. 20c), indicating that the heterogeneity of small pores first increases and then decreases in this process, is beneficial to reduce the heterogeneity of small pores; D_2 remains basically unchanged in the gaseous hydrocarbon production stage (Fig. 20d), indicating that the heterogeneity of large is not affected by gaseous hydrocarbon generation too.

In conclusion, the results of N_2 adsorption show that the heterogeneity of shale pores is strong, pore surface and structure is complex, the liquid hydrocarbon generation process reduces the roughness of small pore surface which may be caused by organic acid dissolution. However, the variation of pore surface roughness is complex in gas production stage, but the final change is small. The heterogeneity of large pore structure is enhanced causing by the hydrocarbon plugging in the oil window. In the gas window, the heterogeneity of pore structure is weakened and the connectivity is improved due to the liquid hydrocarbon cracking to free the space.

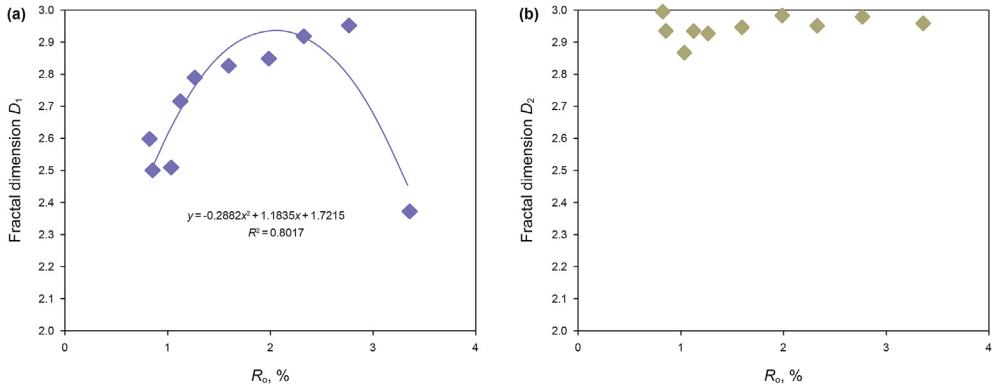

Fig. 19. Relationship between fractal dimension of MICP and R_o.

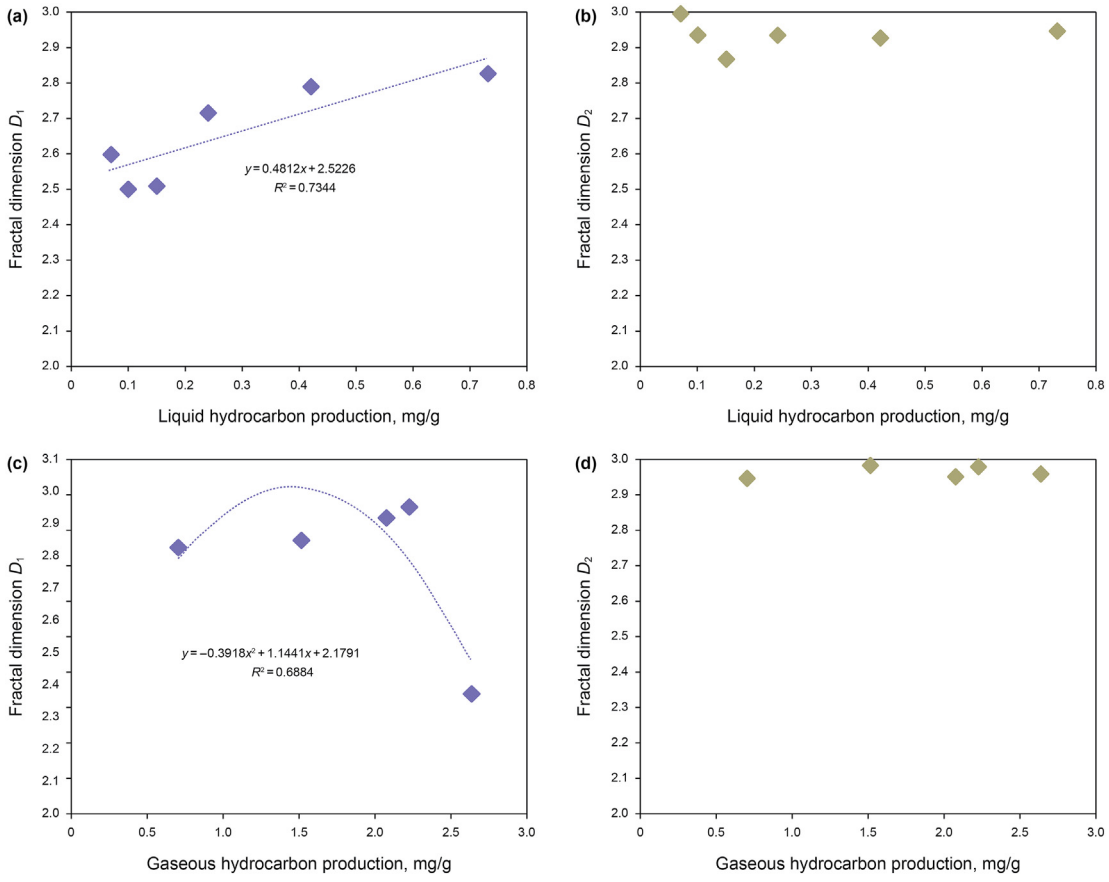

Fig. 20. Relationship between fractal dimension of MICP and the hydrocarbon production.

The fractal dimension of MICP is different from that of N_2 adsorption, which may be caused by the different characterization range of pore. Especially, D_2 of MICP remains basically constant and is closed to 3 in the hydrocarbon generation stage, indicating that the heterogeneity of large pore is great and is not affected by hydrocarbon generation, which is speculated that the heterogeneity of this part of pores is mainly affected by diagenesis.

5. Conclusions

(1) The pore volume and specific surface area of continental shale decrease first and then increase with the increase of R_o during the thermal evolution. This process is conducive to the development of large-pore-size mesopore and macropore, while the pore morphology is not greatly affected by thermal evolution.

(2) The oil generation stage dominated by liquid hydrocarbon (R_o<1.59%) is harmful to the development of micropore, mesopore and macropore. The micropore volume and specific surface area reduce by 82.65% and 78.08% respectively in this stage affected by the transformation of clay minerals. The mesopore volume and specific surface area reduce by 43.45% and 65.6% respectively; the macropore volume reduces by 69.51%. The evolution of mesopore and macropore are mainly affected by the plugging of liquid hydrocarbons and asphaltenes produced by the pyrolysis of OM, and has no obvious relationship with mineral transformation.

(3) In the gas generation stage dominated by gaseous hydrocarbons (1.59% < R_o<3.35%), it is conducive to the development of micropore, mesopore and macropore. In this process, the pore volume of micropore, mesopore and macropore increase by 2.69 times, 2.21 times and 3.2 times respectively, the specific surface area of micropore and macropore increase by 2.45 times and 2.14 times respectively. The evolution of pores in this stage is mainly controlled by the space releasing of liquid hydrocarbon cracking and the transformation of clay minerals. R_o>1.59% is preliminarily defined as a favorable stage for pore development of continental shale.

(4) Hydrocarbon generation has different effects on pore heterogeneity of different scales. For the N_2 adsorption fractal dimension, the roughness of small pore surface (D_1) decreases during the process of oil generation stage, but has no obvious law in the gas generation stage. The complexity of large pores structure (D_2) increases during the liquid hydrocarbon generation stage, but decreases in the gas generation stage; For the MICP fractal dimension, D_1 increases in the liquid hydrocarbon generation stage, and the pore heterogeneity increases, and it increases first and then decreases in the gas generation stage; D_2 remains basically constant during the hydrocarbon generation stage, and is close to 3, indicating that the heterogeneity of large pores is extremely strong and is not affected by thermal evolution hydrocarbon generation.

Acknowledgements

This study was supported by the National Science and Technology Major Project of the Ministry of Science and Technology of China "Study on Formation Mechanism and Enrichment Regularity of Different Types of Shale Gas" (2016ZX05034). The authors thank the Oil & Gas Survey, China Geological Survey for their support of this research.

References

Barrett, E.P., Joyner, L.G., Halenda, P.P., 1951. The determination of pore volume and area distributions in porous substances. I. computations from nitrogen isotherms. J. Am. Chem. Soc. 73 (1), 373–380. https://doi.org/10.1021/ja01145a126.

Brunauer, S., Emmett, P.H., Teller, E., 1938. Adsorption of gases in multimolecular Layers. J. Am. Chem. Soc. 60 (2), 309–319. https://doi.org/10.1021/ja01269a023.

Bu, H., Ju, Y., Tan, J., et al., 2015. Fractal characteristics of pores in nonmarine shales from the Huainan coalfield, eastern China. J. Nat. Gas Sci. Eng. 24, 166–177. https://doi.org/10.1016/j.jngse.2015.03.021.

Chalmers, G.R., Bustin, R.M., Power, I.M., 2012. Characterization of gas shale pore systems by porosimetry, pycnometry, surface area, and field emission scanning electron microscopy/transmission electron microscopy image analyses: examples from the Barnett, Woodford, Haynesville, Marcellus, and Doig unit. AAPG Bull. 96 (6), 1099–1119. https://doi.org/10.1306/10171111052.

Chalmers, G.R.L., Bustin, R.M., 2008. Lower Cretaceous gas shales in Northeastern British Columbia, Part I: geological controls on methane sorption capacity. Bull. Can. Petrol. Geol. 56 (1), 1–21. https://doi.org/10.2113/gscpgbull.56.1.1.

Chen, J., Xiao, X.M., 2014. Evolution of nanoporosity in organic-rich shales during thermal maturation. Fuel 129, 173–181. https://doi.org/10.1016/j.fuel.2014.03.058.

Clarkson, C.R., Solano, N., Bustin, R.M., et al., 2013. Pore structure characterization of North American shale gas reservoirs using USANS/SANS, gas adsorption, and mercury intrusion. Fuel 103, 606–616. https://doi.org/10.1016/j.fuel.2012.06.119.

Cui, J.W., Zou, C.N., Zhu, R.K., et al., 2012. New advances in shale porosity research. Adv. Earth Sci. 27 (12), 1319–1325. https://doi.org/10.11867/j.issn.1001-8166.2012.12.1319 (in Chinese).

Curtis, M.E., Cardott, B.J., Sondergeld, C.H., et al., 2012a. Development of organic porosity in the Woodford Shale with increasing thermal maturity. Int. J. Coal Geol. 103, 26–31. https://doi.org/10.1016/j.coal.2012.08.004.

Curtis, M.E., Sondergeld, C.H., Ambrose, R.J., et al., 2012b. Microstructural investigation of gas shales in two and three dimensions using nanometer-scale resolution imaging. AAPG Bull. 96 (4), 665–667. https://doi.org/10.1306/08151110188.

Dembicki, H.J., Horsfield, B., Ho, T.T.Y., 1983. Source rock evaluation by pyrolysis-gas chromatography. AAPG Bull. 67 (7), 1094–1103. https://doi.org/10.1306/03B5B709-16D1-11D7-8645000102C1865D.

Drummond, C., Israelachvili, J., 2002. Surface forces and wettability. J. Petrol. Sci. Eng. 33 (1–3), 123–133. https://doi.org/10.1016/s0920-4105(01)00180-2.

Dubinin, M.M., Stoeckli, H.F., 1980. Homogeneous and heterogeneous micropore structures in carbonaceous adsorbents. J. Colloid Interface Sci. 75 (1), 34–42. https://doi.org/10.1016/0021-9797(80)90346-X.

Faulon, J.L., Mathews, J.P., Carlson, G.A., et al., 1994. Correlation between microporosity and fractal dimension of bituminous coal based on computer-generated models. Energy Fuels 8 (2), 408–414. https://doi.org/10.1021/ef00044a019.

Fu, J.H., Niu, X.B., Dan, W.D., et al., 2019. The geological characteristics and the progress on exploration and development of shale oil in Chang7 Member of Mesozoic Yanchang Formation, Ordos Basin. China. Petrol. Explor. 24 (5), 601–614. https://doi.org/10.3969/j.issn.1672-7703.2019.05.007 (in Chinese).

Furmann, A., Mastalerz, M., Brassell, S.C., et al., 2013. Extractability of biomarkers from high- and low-vitrinite coals and its effect on the porosity of coal. Int. J. Coal Geol. 107, 141–151. https://doi.org/10.1016/j.coal.2012.09.010.

Gauden, P.A., Terzyk, A.P., Rychlicki, G., 2001. The new correlation between microporosity of strictly microporous activated carbons and fractal dimension on the basis of the Polanyi-Dubinin theory of adsorption. Carbon 39 (2), 267–278. https://doi.org/10.1016/S0008–6223(00)00122-6.

Gu, X., Cole, D.R., Rother, G., et al., 2015. Pores in Marcellus shale: a neutron scattering and FIB-SEM Study. Energy Fuel. 29 (3), 1295–1308. https://doi.org/10.1021/acs.Energyfuels.5b00033.

Guo, H., He, R., Jia, W., et al., 2018. Pore characteristics of lacustrine shale within the oil window in the upper Triassic Yanchang Formation, Southeastern Ordos Basin, China. Mar. Petrol. Geol. 91, 279–296. https://doi.org/10.1016/j.marpetgeo.2018.01.013.

Guo, S.B., Mao, W.J., 2019. Division of diagenesis and pore evolution of a Permian Shanxi shale in the Ordos Basin, China. J. Petrol. Sci. Eng. 182, 351–360. https://doi.org/10.1016/j.petrol.2019.106351.

Hu, H., Hao, F., Lin, J., et al., 2017. Organic matter-hosted pore system in the Wufeng-Longmaxi (O_3w-S_{11}) shale, Jiaoshiba area, eastern Sichuan basin, China. Int. J. Coal Geol. 173, 40–50. https://doi.org/10.1016/j.coal.2017.02.004.

Jarvie, D.M., Hill, R.J., Ruble, T.E., et al., 2007. Unconventional shale-gas systems: the Mississippian Barnett Shale of north Central Texas as one model for thermogenic shale-gas assessment. AAPG Bull. 91 (4), 475–499. https://doi.org/10.1306/12190606068.

Ko, L.T., Ruppel, S.C., Loucks, R.G., et al., 2018. Pore-types and pore-network evolution in Upper Devonian-lower Mississippian Woodford and Mississippian Barnett mudstones: insights from laboratory thermal maturation and organic petrology. Int. J. Coal Geol. 190, 3–28. https://doi.org/10.1016/j.coal.2017.10.001.

Li, J.J., Yin, J.X., Zhang, Y.N., et al., 2015. A comparison of experimental methods for describing shale pore features - a case study in the Bohai Bay Basin of eastern China. Int. J. Coal Geol. 152, 39–49. https://doi.org/10.1016/j.coal.2015.10.009.

Lin, W., Mastalerz, M., Schimmelmann, A., et al., 2014. Influence of Soxhlet-extractable bitumen and oil on porosity in thermally maturing organic-rich shales. Int. J. Coal Geol. 132, 38–50. https://doi.org/10.1016/j.coal.2014.08.003.

Loucks, R.G., Reed, R.M., Ruppel, S.C., et al., 2009. Morphology, genesis, and distribution of nanometer-scale pores in siliceous mudstones of the Mississippian Barnett Shale. J. Sediment. Res. 79 (11), 848–861. https://doi.org/10.2110/jsr.2009.092.

Ma, Z.L., Zheng, L.J., Xu, X.H., et al., 2017. Thermal simulation experiment of organic matter-rich shale and implication for organic pore formation and evolution. Petrol. Res. 2 (4), 347–354. https://doi.org/10.1016/j.ptlrs.2017.04.005.

Mastalerz, M., Schimmelmann, A., Drobniak, A., et al., 2013. Porosity of Devonian and Mississippian New Albany Shale across a maturation gradient: insights from organic petrology, gas adsorption, and mercury intrusion. AAPG Bull. 97 (10), 1621–1643. https://doi.org/10.1306/04011312194.

Mathia, E.J., Bowen, L., Thomas, K.M., et al., 2016. Evolution of porosity and pore types in organic-rich, calcareous, Lower Toarcian Posidonia Shale. Mar. Petrol. Geol. 75, 117–139. https://doi.org/10.1016/j.marpetgeo.2016.04.009.

Milliken, K.L., Rudnicki, M., Awwiller, D.N., et al., 2013. Organic matter hosted pore system, Marcellus Formation (Devonian), Pennsylvania. AAPG Bull. 97 (2), 177–200. https://doi.org/10.1306/07231212048.

Modica, C.J., Lapierre, S.G., 2012. Estimation of kerogen porosity in source rocks as a function of thermal transformation: example from the Mowry Shale in the Powder River Basin of Wyoming. AAPG Bull. 96 (1), 87–108. https://doi.org/10.1306/04111110201.

Peng, Y.X., Guo, S.B., Zhai, G.Y., et al., 2019. Determination of critical parameters for evaluating coal measure shale gas in China. Mar. Petrol. Geol. 109, 732–739. https://doi.org/10.1016/j.marpetgeo.2019.06.017.

Pfeifer, P., Wu, Y.J., Cole, M.W., et al., 1989. Multilayer adsorption on a fractally rough surface. Phys. Rev. Lett. 62 (17), 1997–2000. https://doi.org/10.1103/PhysRevLett.62.1997.

Pommer, M., Milliken, K., 2015. Pore types and pore-size distributions across thermal maturity, Eagle Ford Formation, southern Texas. AAPG Bull. 99 (9), 1713–1744. https://doi.org/10.1306/03051514151.

Ross, D.J.K., Bustin, R.M., 2007. Impact of mass balance calculations on adsorption capacities in microporous shale gas reservoirs. Fuel 86, 2696–2706. https://doi.org/10.1016/j.fuel.2007.02.036.

Ross, D.J.K., Bustin, R.M., 2009. The importance of shale composition and pore structure upon gas storage potential of shale gas reservoirs. Mar. Petrol. Geol. 26 (6), 916–927. https://doi.org/10.1016/j.marpetgeo.2008.06.004.

Sing, K.S.W., Everett, D.H., Haul, R.A.W., et al., 1985. Reporting physisorption data for gas/solid systems with special reference to the determination of surface area and porosity. Pure Appl. Chem. 57, 603–619. https://doi.org/10.1351/pac198557040603.

Sun, L.N., Tuo, J.C., Zhang, M.F., et al., 2015. Formation and development of the pore structure in Chang 7 member oil-shale from Ordos Basin during organic matter evolution induced by hydrous pyrolysis. Fuel 158, 549–557. https://doi.org/10.1016/j.fuel.2015.05.061.

Tang, X., Zhang, J.C., Ding, W.L., 2016. The reservoir property of the Upper Paleozoic marine-continental transitional shale and its gas-bearing capacity in the Southeastern Ordos Basin. Earth Sci. Front. 23 (2), 147–157. https://doi.org/10.13745/j.esf.2016.02.015 (in Chinese).

Valenza, J.J., Drenzek, N., Marques, F., et al., 2013. Geochemical controls on shale microstructure. Geology 41 (5), 611–614. https://doi.org/10.1130/G33639.1.

Wang, F.T., Guo, S.B., 2019. Influential factors and model of shale pore evolution: a case study of a continental shale from the Ordos Basin. Mar. Petrol. Geol. 102, 271–282. https://doi.org/10.1016/j.marpetgeo.2018.12.045.

Wang, M., Xue, H., Tian, S., et al., 2015. Fractal characteristics of upper Cretaceous lacustrine shale from the Songliao Basin, NE China. Mar. Petrol. Geol. 67, 144–153. https://doi.org/10.1016/j.marpetgeo.2015.05.011.

Wang, S.J., Li, D.H., Li, J.Z., 2011. Exploration potential analysis of shale gas in the Ordos Basin. Nat. Gas. Ind. 12, 40–46. https://doi.org/10.3787/j.issn.1000-0976.2011.12.006 (in Chinese).

Wu, F.L., Li, W.H., Li, Y.H., et al., 2004. Delta sediments and evolution of the Yanchang Formation of upper Triassic in Ordos Basin. J. Palaeogeogr. 6 (3), 307–314. https://doi.org/10.1007/BF02873097.

Xie, D.L., Guo, H.Y., Zhao, D.P., 2014. Fractal characteristics of adsorption pore of shale based on low temperature nitrogen experiment. J. China Coal Soc. 39 (12), 2466–2472. https://doi.org/10.13225/j.cnki.jccs.2013.1825 (in Chinese).

Yang, F., Ning, Z., Liu, H., 2014. Fractal characteristics of shales from a shale gas reservoir in the Sichuan Basin, China. Fuel 115, 378–384. https://doi.org/10.1016/j.fuel.2013.07.040.

Yang, H., Deng, X.Q., 2013. Deposition of Yanchang Formation deep-water sandstone under the control of tectonic events, Ordos Basin. Petrol. Explor. Dev. 40 (5), 513–520. https://doi.org/10.1016/S1876-3804(13)60072-5.

Yao, B.Y., Li, D.P., 2013. Determination conditions and measured value analysis of vitrinite reflectance. Coal Geol. Explor. 41 (5), 11–16. https://doi.org/10.3969/j.issn.1001-1986.2013.05.003 (in Chinese).

Yao, Y.B., Liu, D.M., Tang, D.Z., et al., 2008. Fractal characterization of adsorption-pores of coals from North China: an investigation on CH_4 adsorption capacity of coals. Int. J. Coal Geol. 73 (1), 27–42. https://doi.org/10.1016/j.coal.2007.07.003.

Zhao, K.Y., Guo, S.B., 2015. Characteristics and main controlling factors of shale gas reservoirs in transitional facies: a case study of Upper Paleozoic in Ordos Basin. Petrol. Geol. Exp. 37 (2), 141–149. https://doi.org/10.7603/s40972-015-0023-5 (in Chinese).

Zhao, X.Y., He, D.B., 2012. Clay minerals and shale gas. Xinjing Pet. Geol. 33 (6), 643–647. https://doi.org/10.7657/XJPG20210401 (in Chinese).